Int J Earth Sci (Geol Rundsch) (2007) 96:1179–1194
DOI 10.1007/s00531-006-0146-y

ORIGINAL PAPER

Zircon age and Nd–Hf isotopic composition of the Yunnan Tethyan belt, southwestern China

Fukun Chen · Xiang-Hui Li · Xiu-Li Wang · Qiu-Li Li · Wolfgang Siebel

Received: 5 June 2006 / Accepted: 16 November 2006 / Published online: 8 December 2006

Abstract The Baoshan block of the Tethyan Yunnan, southwestern China, is considered as northern part of the Sibumasu microcontinent. Basement of this block that comprises presumably greenschist-facies Neoproterozoic metamorphic rocks is covered by Paleozoic to Mesozoic low-grade metamorphic sedimentary rocks. This study presents zircon ages and Nd–Hf isotopic composition of granites generated from crustal reworking to reveal geochemical feature of the underlying basement. Dating results obtained using the single zircon U–Pb isotopic dilution method show that granites exposed in the study area formed in early Paleozoic (about 470 Ma; Pingdajie granite) and in late Yanshanian (about 78–61 Ma, Late Cretaceous to Early Tertiary; Huataolin granite). The early Paleozoic granite contains Archean to Mesoproterozoic inherited zircons and the late Yanshanian granite contains late Proterozoic to early Paleozoic zircon cores. Both granites have similar geochemical and Nd–Hf isotopic charateristics, indicating similar magma sources. They have whole-rock T_{DM}(Nd) values of around 2,000 Ma and zircon T_{DM}(Hf) values clustering around 1,900–1,800 and 1,600–1,400 Ma. The Nd–Hf isotopic data imply Paleoproterozoic to Mesoproterozoic crustal material as the major components of the underlying basement, being consistent with a derivation from Archean and Paleoproterozoic terrains of India or NW Australia. Both granites formed in two different tectonic events similarly originated from intra-crustal reworking. Temporally, the late Yanshanian magmatism is probably related to the closure of the Neotethys ocean. The early Paleozoic magmatism traced in the Baoshan block indicates a comparable history of the basements during early Paleozoic between the SE Asia and the western Tethyan belt, such as the basement outcrops in the Alpine belt and probably in the European Variscides that are considered as continental blocks drifting from Gondwana prior to or simultaneously with those of the SE Asia.

Keywords Early Paleozoic · Granite · Nd–Hf isotope · Tethys · Yunnan · Zircon age

F. Chen (✉)
State Key Laboratory of Lithospheric Evolution,
Institute of Geology and Geophysics,
Chinese Academy of Sciences, Beijing 100029, China
e-mail: fukun-chen@mail.igcas.ac.cn

F. Chen · X.-H. Li · X.-L. Wang · Q.-L. Li
Laboratory for Radiogenic Isotope Geochemistry,
Institute of Geology and Geophysics,
Chinese Academy of Sciences, Beijing 100029, China

W. Siebel
Institut für Geowissenschaften,
Universität Tübingen, 72074 Tübingen, Germany

Introduction

Western Yunnan, usually interpreted as the southeastern part of the Himalayan belt, belongs to one of the important branches of the eastern Tethyan tectonic belt and, therefore, bears significance of the Tethyan belt in SE Asia (e.g., Gansser 1981; Tapponier et al. 1981; Sengör 1988). Geological evolution of SE Asia from Paleozoic to Mesozoic can be regarded as an accretion history by the amalgamation of several micro-continents or continental blocks to the Eurasian supercontinent due to successive closure of Tethys oceans (e.g., Sengör 1988). In common view, these mirco-continents rifted from the northern margin of

supercontinent Gondwana and drifted northwards (e.g., Metcalfe 1996a, b; Ueno 2000). The Tethyian orogen of western Yunnan is composed of several continental blocks (terranes) and suture zones, e.g., the Simao, Tengchong and Baoshan blocks and the Changning-Menglian suture zone (e.g., Zhong 1998).

According to the distribution of the Jurassic fauna, Neumayr (1885) developed the idea that during the Mesozoic an ocean traversing the Eurasian continent must have existed along the equator. Suess (1893) proposed that such an ocean which he named ''Tethys'' separated Laurentia in the north from Gondwana in the south. Closure of the Tethys and subsequently collision of these two continents built the Alpine-Himalayan orogenic belt. Further studies on the Tethyan belt and paleogeographical reconstruction of continents have revealed the existence of the Paleo-Tethys in the east of the Pangea supercontinent during the Carboniferous to Permian time (e.g., Sengör 1988; Sengör and Natal'in 1996). Consequently, it has been commonly accepted that at least two ocean basins, the Paleo-Tethys and the Neotethys, were closed before the final collision of Gondwana and Laurentia (e.g., Sengör 1988). Metcalfe (1996a, b, 2002) has proposed the existence of a Meso-Tethys ocean basin that was opened in late Early Permian and closed before Late Cretaceous times. Between Gondwana and Laurentia, numerous micro-continents or continental blocks, such as Cimmeria (Sengör 1988), Sibumasu, and the Lhasa block (e.g., Metcalfe 1996a, b; Jin 2002; Wang et al. 2001), were rifted from the northern margin of Gondwana and were subsequently accreted to the Eurasian continent during the Paleozoic and Mesozoic (Metcalfe 1996a, b; Ueno 2000). Besides biogeographical constraints, provenance analysis of the basements of these micro-continents is crucial for understanding the origin and tectonic processes, which led to the formation of the Tethyan orogenic belt. Basement rocks in the Yunnan Tethyan belt are generally concealed beneath thick cover sequences. This study aims to obtain indirect evidence from granites derived from the underlying basement. Here we present zircon ages and Hf isotopic composition as well as geochemical and Nd isotopic data of granites exposed in the Baoshan block to constrain the age and isotopic characteristics of this block and to discuss the pre-Tethyan evolution of Tethyan Yunnan.

Geological setting

The Tethyan belt in the western Yunnan (Fig. 1a) comprises the Simao block of South China affinity and the Baoshan and Tengchong blocks of Gondwana affinity (Wu et al. 1995; Metcalfe 1996a, b; Wopfner 1996; Zhong 1998; Ueno 2000). The last two blocks belong to the northern part of the Sibumasu micro-continent (Metcalfe 1988, 1996a, b, 1998) or the Shan-Thai block (e.g., Hutchison 1993; Shi and Archbold 1995, 1998). During the Triassic closure of the Changning-Menglian ocean, a branch of the Paleo-Tethys, these two micro-continental blocks formed different tectonic entities along the passive continental margin of Gondwanaland. Some researchers consider that they were separated by the eastern branch of the Banggong-Nujiang ocean basin that formed during the development of the Neotethys. This ocean basin was closed in early Jurassic and, subsequently, the Tengchong and Baoshan blocks were welded together (e.g., Zhong 1998). The collision led to the formation of the Gaoligongshan high-grade metamorphic zone.

In its present position, the Tengchong and Baoshan blocks are separated by the Lushui-Luxi-Ruili fault (LLRF). The basement is largely covered by medium-grade to low-grade metamorphic clastic Paleozoic to early Mesozoic sedimentary rocks. These rocks are intruded by numerous granitoids mainly Mesozoic to Cenozoic in age (Yunnan Geological Survey 1981; Zhong 1998). The Mesozoic granitoids are probably related to subduction of the Neotethys before the Indo-Eurasian collision, whereas the Cenozoic granitoids post-date the Indo-Eurasian collision (e.g., Rowley 1996). In the Tengchong block, rift-related volcanism was active over the last five million years. Volcanic rocks are basaltic to andesitic in composition and were derived from a metasomatized mantle source that probably resulted from prior subduction beneath Asia (e.g., Zhu et al. 1983; Chen et al. 2002a). The basement of the Tengchong block, also interpreted as the southeastern part of the Himalayan fold zone or part of the Sundaland plate (e.g., Fan 1978; Powell and Johnson 1980), is mainly composed of gneiss, migmatite, migmatitic granite, and small lenses of mafic rocks. The Gaoligongshan metamorphic zone comprises diverse rock types of different ages, including migmatitic granites, probably being Cenozoic in age, low-grade metasediments, supposed to be early Paleozoic in age, and amphibolite-facies orthogneisses which have Mesoproterozoic to Neoproterozoic protolith ages (Yunnan Geological Survey 1981). Orthogneisses are probably part of the basement of the Gondwana-affinity blocks. The basement of the Baoshan block is largely hidden by young sedimentary cover rocks. It is commonly accepted that the Pake Group of the Ximeng rock complex represents part of the Baoshan basement. Rocks of this group which underwent

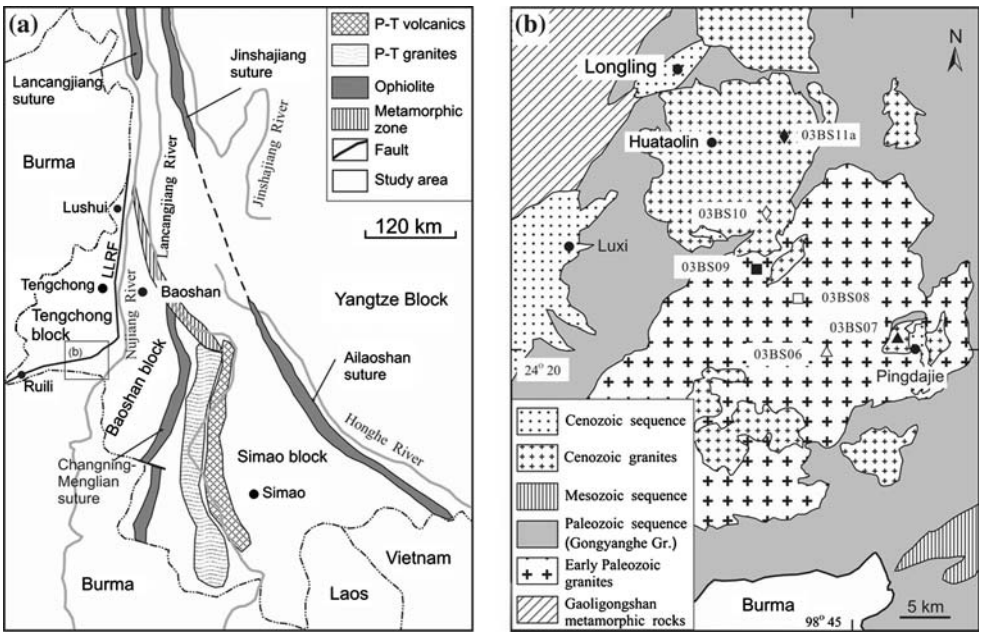

Fig. 1 **a** Geological sketch of the Tethyan belt in western Yunnan (Zhong 1998). **b** Geological map of the study area (Yunnan Geological Survey 1981) showing the sample locality. *LLRF* the Lushui-Luxi-Ruili fault

greenschist-facies metamorphism are Neoproterozoic in age (e.g., Zhong 1998).

A sedimentary rock unit, known as the Gongyanghe Group of late Precambrian (?) to early Cambrian age is exposed in the study area (Fig. 1b). It was formerly considered as part of the basement of the Baoshan block in this area. This group is mainly composed of low-grade metamorphic arkose, sandstone and silt slate in the lower part and contains silicalite layers in the upper part. The thickness and number of the silicalite layers increases upwards. The Gongyanghe Group is bounded to the high-grade metamorphic rocks of the Tengchong block in the northwest by the Lushui-Luxi-Ruili fault. Paleozoic and late Mesozoic to early Cenozoic granites intruded into this group that is partly covered by late Cambrian to Cenozoic sedimentary rocks. Six analyzed samples whose localities are shown in Fig. 1b were collected from the early Paleozoic Pingdajie granite (samples 03BS06, 03BS08 and 03BS09) and from the Huataolin granite of late Mesozoic to early Cenozoic age (samples 03BS07, 03BS10 and 03BS11a). In Chinese literatures, the Huataolin granite belongs to the late Yanshanian (Late Cretaceous to Early Tertiary) magmatic cycle.

Analytical methods

Whole-rock powder was obtained by crushing and splitting of about 15 kg of rock material. Zircons were isolated from crushed rocks by standard mineral separation techniques and were finally handpicked for analysis under a binocular microscope. For cathodoluminescence (CL) investigation zircon grains were mounted in epoxy resin and polished down to expose the grain centres. CL images were obtained on a microprobe CAMECA SX51 at the Institute of Geology and Geophysics, Chinese Academy of Sciences (IGG CAS). Zircon U–Pb analysis was performed on a Finnigan MAT-262 at Tübingen University, Germany, and on a GV IsoProbe-T mass spectrometer at the Laboratory for Radiogenic Isotope Geochemistry (LRIG), IGG CAS. Sm–Nd and Rb–Sr isotopic composition was measured using a Finnigan MAT-262 mass spectrometer at the LRIG. Major element contents were analyzed by the X-ray fluorescence spectrometry (XRF) with a Philips PW1400 spectrometer at the IGG CAS. Trace element contents were measured by an inductively coupled plasma mass spectrometry (ICP-MS; Finnigan MAT Element) at the IGG CAS. Analytical uncertainties are generally better than 5%.

For conventional U–Pb isotopic dilution analyses, single zircons or populations consisting of a few morphological identical grains (up to four grains) were shortly washed in warm 7 N HNO_3 and warm 6 N HCl prior to dissolution to remove surface contamination after air abrasion (Krogh 1982). A mixed ^{205}Pb–^{235}U-tracer solution was added to the grain(s). Dissolution was performed in PTFE vessels in a Parr acid digestion bomb (Parrish 1987) using the vapor digestion method. The bomb was placed in an oven at 210°C for 1 week in 22N HF acid and for 1 day in 6 N HCl acid to dissolve fluorides into chloride salts and avoid U–Pb fraction-

ation. Separation of U and Pb was carried out by ion exchange chromography using Teflon columns filled with 40-μl AG1-X8 (100–200 mesh) anion exchange resin. The separation procedure is described in Poller et al. (1997). Intensity of ^{204}Pb was measured on the ion counter when using the MAT262 mass spectrometer or the Daly detector of the IsoProbe-T mass spectrometer, while other Pb isotopes were measured with Faraday cups. Total procedural blanks were <10 pg for Pb and U. A factor of 1‰ per atomic mass unit for instrumental mass fractionation was applied to all Pb analyses, using NBS 981 as reference material. Common Pb contribution remaining after correction for tracer and blank was corrected using values of Stacey and Kramers (1975). U–Pb analytical data were evaluated using the Pbdat program (Ludwig 1988). More details on analytical techniques are given in Chen et al. (2000, 2002c). Results of in house measurements on natural zircons from the Phalaborwa Igneous Complex/South Africa and from Kuehl Lake/Canada (Zircon 91500; Wiedenbeck et al. 1995) are summarized in Chen et al. (2002b). Using the U–Pb method, we obtained a ^{207}Pb/^{206}Pb age of 2053.5 ± 1.2 Ma for Phalaborwa zircon, similar to the age of 2051.8 ± 0.4 Ma obtained by the evaporation method (Kröner et al. 2001). Analysis of zircon 91500 gave nearly concordant U–Pb ages of 1065.6 ± 2.2 Ma, consistent with the reported U–Pb age of 1065.4 ± 0.3 Ma obtained in different laboratories (Wiedenbeck et al. 1995). Pb evaporation ages are expressed as a weighted average of ^{207}Pb/^{206}Pb ratios and the errors refer to the 95% confidence level, calculated using the Isoplot program (Ludwig 2001).

For Nd–Sr isotope analyses, Rb–Sr and light rare-earth elements were isolated on quartz columns by conventional ion exchange chromatography with a 5-ml resin bed of AG 50W-X12 (200–400 mesh). Nd and Sm were separated from other rare-earth elements on quartz columns using 1.7-ml Teflon powder coated with HDEHP, di(2-ethylhexyl)orthophosphoric acid, as cation exchange medium. Sr was loaded with a Ta–HF activator on pre-conditioned W filaments and was measured in single-filament mode. Nd was loaded as phosphate on pre-conditioned Re filaments and measurements were performed in a Re double filament configuration. The ^{87}Sr/^{86}Sr and ^{143}Nd/^{144}Nd ratios are normalized to ^{86}Sr/^{88}Sr = 0.1194 and ^{146}Nd/^{144}Nd = 0.7219, respectively. In the LRIG, repeated measurements of Ames metal and the NBS987 Sr standard during the 2004/2005 period gave mean values of 0.512149 ± 0.000022 (n = 98) for the ^{143}Nd/^{144}Nd ratio and 0.710244 ± 0.000033 (n = 100) for the ^{87}Sr/^{86}Sr ratio. Results of repeated Rb–Sr and Sm–Nd analyses on the standard material BCR-1 (basalt powder) are given in Table 2. The external precision refers to the 2σ uncertainty based on replicate measurements on these standard solutions over 1 year. Total procedural blanks were <300 pg for Sr and <50 pg for Nd.

In situ zircon Hf isotopic composition was measured on a Finnigan Neptune Multi-Collector ICP-MS at the MC-ICP-MS laboratory, IGG CAS. The laser system delivers a beam of 193 nm UV light from a Geolas excimer laser ablation system. Sampling spots have beam diameters of 63 or 32 μm for small grains. Ar and He carrier gases were used to transport the ions derived from the ablated material in the laser-ablation cell via a mixing chamber to the ICP-MS torch. For details on measurement procedures and interference correction see Xu et al. (2004). Isotope analyses were performed on those zircons monitored by CL studies, and the CL images provided guidance in the choice of the beam spot site. Isobaric interference of ^{176}Lu on ^{176}Hf was corrected using the intensity of the interference-free ^{175}Lu isotope and a recommended ^{176}Lu/^{175}Lu ratio of 0.02655 (Machado and Simoetti 2001), while isobaric interference of ^{176}Yb on ^{176}Hf isotope was corrected using the interference-free ^{172}Yb isotope and a recommended ^{176}Yb/^{172}Yb ratio of 0.5886 (Chu et al. 2002). Zircon 91500 was used as the reference standard during routine analyses, with a recommended ^{176}Hf/^{177}Hf ratio of 0.282293 ± 28 from laser analyses (Woodhead et al. 2004). $\varepsilon_{Hf}(t)$ values were calculated using chondritic Hf data (Blichert-Toft and Albarede 1997). Parameters used for calculation of depleted mantle model ages (T_{DM}(Hf)) are from Griffin et al. (2000).

Chemical and Nd–Sr isotopic composition

Three analysed samples collected from the early Paleozoic Pingdajie granite are fine-grained biotite granites, containing quartz, feldspar and biotite as major mineral constituents with minor secondary muscovite, apatite, zircon and opaque phases. Three samples of the late Yanshanian Huataolin granite are medium-grained granites containing mainly quartz and feldspar, and minor biotite and muscovite. Accessory minerals are zircon, apatite and opaque phases. Sample 03BS11a is a light colored tourmaline-bearing rock.

Analytical data for major and trace elements of six whole-rock samples are given in Table 1. SiO_2 and Al_2O_3 contents range from 71.2 to 77.0 and 12.6 to 16.7 wt%, respectively. A/CNK values (molar Al_2O_3/($CaO + Na_2O + K_2O$) ratio) vary from 1.14 to 1.49 (Fig. 2a), indicating peraluminous composition

Table 1 Major and trace element concentrations of granites from the Baoshan block

Sample	03BS06	03BS08	03BS09	03BS07	03BS10	03BS11a
SiO_2	71.79	72.06	73.41	76.98	71.36	71.16
TiO_2	0.33	0.28	0.11	0.04	0.18	0.03
Al_2O_3	14.31	14.37	14.57	12.65	15.19	16.68
Fe_2O_3	3.29	2.85	1.18	0.96	1.27	0.45
MnO	0.07	0.06	0.04	0.13	0.04	0.04
MgO	1.47	1.58	0.28	0.18	0.33	0.09
CaO	0.42	0.35	0.69	0.48	1.08	0.06
Na_2O	4.20	4.57	3.28	3.26	3.44	4.24
K_2O	1.81	2.46	4.75	4.48	5.02	3.92
P_2O_5	0.12	0.08	0.19	0.07	0.17	0.39
LOI	1.73	1.30	0.88	0.73	1.43	2.38
Total	99.54	99.96	99.38	99.97	99.51	99.45
Ba	209	189	195	32	311	6.6
Cs	3.0	23	28	16	26	49
Nb	16.1	19.0	15.6	17.8	23.6	38.3
Ni	2.2	17	4.3	2.1	3.6	2.6
Rb	115	185	308	484	411	695
Sr	47	33	47	9.7	80	9.2
Y	23	16	11	17	8.1	2.5
Zr	173	119	47	32	94	13
Hf	16	19	16	18	24	38
Pb	9.9	5.8	38	33	42	15
Th	17	22	6.0	7.9	25	1.2
U	4.0	5.6	3.6	16	22	1.7
La	34.0	24.8	11.9	5.84	31.2	1.63
Ce	69.3	50.4	25.4	11.9	56.2	2.21
Pr	8.02	5.86	2.99	1.75	7.10	0.37
Nd	29.6	22.3	10.9	6.25	24.3	1.21
Sm	5.98	4.45	2.89	2.19	4.47	0.43
Eu	0.81	0.56	0.44	0.06	0.51	0.02
Gd	5.26	3.74	3.09	2.23	3.01	0.43
Tb	0.79	0.57	0.51	0.49	0.39	0.11
Dy	4.38	3.18	2.45	3.22	1.78	0.75
Ho	0.90	0.64	0.40	0.65	0.29	0.12
Er	2.46	1.83	0.91	1.95	0.77	0.29
Tm	0.36	0.27	0.12	0.35	0.10	0.04
Yb	2.37	1.75	0.77	2.43	0.62	0.29
Lu	0.34	0.27	0.10	0.38	0.09	0.04
$\sum_{REE}$	164.6	120.6	62.9	39.4	131.1	7.94
A/CNK	1.49	1.34	1.24	1.14	1.16	1.47
$(La/Yb)_N$	9.6	9.5	10.3	1.6	33.6	3.8
$(Tb/Yb)_N$	1.47	1.44	2.93	0.89	2.78	1.68
Eu/Eu*	0.44	0.42	0.45	0.08	0.43	0.14

Contents of major and trace elements are given in wt% and in ppm, respectively

A/CNK molar ratio $Al_2O_3/(CaO + Na_2O + K_2O)$, *Eu/Eu** $(Eu)_N/((Sm)_N*(Gd)_N)^{1/2}$, *Samples 03BS06, 03BS08* and *03BS09* early Paleozoic Pingdajie granite, *Samples 03BS07, 03BS10* and *03BS11a* late Yanshanian Huataolin granite

(Fig. 2b). The samples are characterized by high Rb/Sr ratios and plot in or close to the field of syn-collisional granites in the (Y+Nb) versus Rb diagram (Fig. 3). The three samples from the Pingdajie granite exhibit similar chondrite-normalised rare earth element (REE) patterns with moderate light over heavy REE enrichment (normalised La/Yb ratios 9.5–10.3; normalised Tb/Yb ratio 1.44–2.93) and negative Eu-anomalies (Eu/Eu* 0.42–0.45) (Fig. 4a). The three samples from the Huataolin granite have low and variable REE contents (Σ_{REE} 131.1–7.94 ppm) and distinct negative Eu-anomalies (Eu/Eu* 0.08–0.43). The flat REE pattern of two of these samples (Fig. 4b) is likely the result of fractionation of LREE-rich accessory phases. A stronger degree of differentiation is also indicated by the high Rb/Sr ratios of these samples. Normalised La/Yb and Tb/Yb ratios range from 1.6 to 33.6 and from 0.89 to 2.78, respectively. Both the Pingdajie and Huataolin granites have similar mantle-normalised multi-element patterns (Fig. 4c, d), that show negative Nb, Sr and Ti and positive Pb anomalies characteristic of the continental crust.

Analytical results of whole-rock Rb–Sr and Sm–Nd isotopic composition of six samples are given in Table 2. Due to their chemical differentiation, the analysed samples display high $^{87}Rb/^{86}Sr$ ratios and, as a consequence, calculated initial $^{87}Sr/^{86}Sr$ ratios show a large variation. When calculated back to 470 Ma, initial ε_{Nd} values of the early Paleozoic Pingdajie granites range from –9.1 to –11.5, depleted-mantle modal ages,

Table 2 Analytical data of whole-rock Rb–Sr and Sm–Nd isotopic composition

Sample	Rb (ppm)	Sr (ppm)	$^{87}Rb/^{86}Sr$	$^{87}Sr/^{86}Sr$ (2σ)	$^{87}Sr/^{86}Sr(t)$	Sm	Nd	$^{147}Sm/^{144}Nd$	$^{143}Nd/^{144}Nd$ (2σ)	$^{143}Nd/^{144}Nd(t)$ t = 470 Ma	$\varepsilon\ \varepsilon_N d(t)$ t = 470 Ma	T_{DM} (Ga)
Pingdajie granite (470 Ma)												
03BS06	115.5	51.51	6.518	0.757802 ± 12	0.71416 ± 22	6.143	29.99	0.1240	0.511947 ± 10	0.511565 ± 22	–9.12 ± 0.42	1.97
03BS08	193.2	37.00	15.18	0.760710 ± 15	<0.7	4.871	23.24	0.1269	0.511956 ± 14	0.511565 ± 24	–9.11 ± 0.47	1.97
03BS09	245.9	42.21	17.08	0.843572 ± 14	0.72920 ± 58	3.427	12.58	0.1649	0.511952 ± 12	0.511444 ± 28	–11.48 ± 0.55	2.16
Huataolin granite (65 Ma)												
03BS07	488.0	11.55	132.4	1.556512 ± 23	1.44366 ± 58	2.801	8.293	0.2045	0.512199 ± 14	0.511569 ± 35	–9.03 ± 0.67	1.96
03BS10	395.7	89.93	12.90	0.735949 ± 13	0.72495 ± 6	4.921	25.68	0.1160	0.511946 ± 13	0.511589 ± 22	–8.65 ± 0.43	1.93
03BS11a	673.2	11.44	172.6	0.865060 ± 19	0.71794 ± 75	0.526	1.640	0.1942	0.512191 ± 50	0.511593 ± 58	–8.57 ± 1.14	1.92
Standard material												
BCR-1	46.54	329.5	0.4066	0.705027 ± 74	(n = 36)	6.676	28.77	0.1405	0.512633 ± 35	(n = 45)		

Initial $^{87}Sr/^{86}$ Sr ratios were calculated for 470 Ma (Pingdajie granite) and 65 Ma (Yanshanian Huataolin granite). Initial $^{143}Nd/^{144}$ Nd ratios and initial ε_{Nd} values were calculated back to 470 Ma for both the Early Paleozoic and the late Yanshanian granites. Errors of initial ratios are propagated from the uncertainties of measured isotopic ratios, element contents and ages. T_{DM} values are two-stage depleted-mantle model ages, using t = 470 Ma, $^{147}Sm/^{144}Nd$ = 0.12 for samples, and $^{147}Sm/^{144}$ Nd = 0.2137 and $^{143}Nd/^{144}Nd$ = 0.51315 for depleted mantle. BCR-1: standard material of basalt powder. Results of standard material BCR-1 were obtained during the 2004/2005 period in the Laboratory for Radiogenic Isotope Geochemistry, Institute of Geology and Geophysics, Chinese Academy of Sciences

using a two-stage model (Liew and Hofmann 1988), range from 1.9 to 2.16 Ga. Irrespective of the different REE pattern, the late Yanshanian Huataolin granite has similar ε_{Nd} (470 Ma) values (–8.57 to –9.03) and similar two-stage modal ages (1.93–1.96 Ga) as the Pingdajie granite (Fig. 5). With respect to these data, both granites might have been derived from similar magma sources.

Zircon ages and Hf isotopic composition

Internal structures of typical zircon populations were studied using the cathodoluminescence (CL) technique prior to U–Pb and Hf isotopic analyses. Zircons of the Pingdajie and Huataolin granites have magmatic habitus (Fig. 6). Most grains of samples 03BS06, 03BS09 and 03BS10 show oscillatory zoning indicative of igneous crystallization (e.g., Hanchar and Miller 1993; Pidgeon et al. 1998). The grains do not show solid-state recrystallization textures or metamorphic-related overgrowth, which would indicate post-crystallization processes. Some zircon grains of samples 03BS06 and 03BS09 contain inherited cores with weak oscillatory CL zoning. Sample 03BS10 largely contains zircon grains having distinguishable cores. Zircon grains of sample 03BS11a exhibit a multitude of CL features. Most grains from this sample do not show typical oscillatory zoning but show sponge-like CL textures.

Two samples of the Pingdajie granite (03BS06, 03BS09) and two samples of the Huataolin granite (03BS10, 03BS11a) were analyzed by the single zircon U–Pb isotopic dilution method. Anaytical data for 43 zircon fractions are given in Table 3 and shown in concordia diagrams in Fig. 7. Eight out of thirteen zircon fractions of sample 03BS06 plot on or close to the concordia around 470 Ma, giving a mean $^{206}Pb/^{238}U$ age of 472 ± 5 Ma. One fraction yields younger discordant U–Pb ages of about 400 Ma, indicating partial Pb-loss. The other four zircon grains contain inherited cores probably as old as Archean in age (upper intercept at 2950 ± 300 Ma; Fig. 7a). Similarly, seven zircon grains of sample 03BS09 yield near concordant U–Pb ages around 470 Ma, with a mean $^{206}Pb/^{238}U$ age of 466 ± 11 Ma. This sample contains old inherited zircon components of Archean to Mesoproterozoic age (upper intercepts at 3580 ± 380 Ma and 1350 ± 130 Ma; Fig. 7b). Two zircon fractions gave nearly concordant U–Pb ages around 520 Ma, likely representing the contribution of younger crustal material to the magma source. Most zircon grains of sample 03BS10 gave discordant U–Pb ages (Fig. 7c), consistent with the internal zircon structure shown in

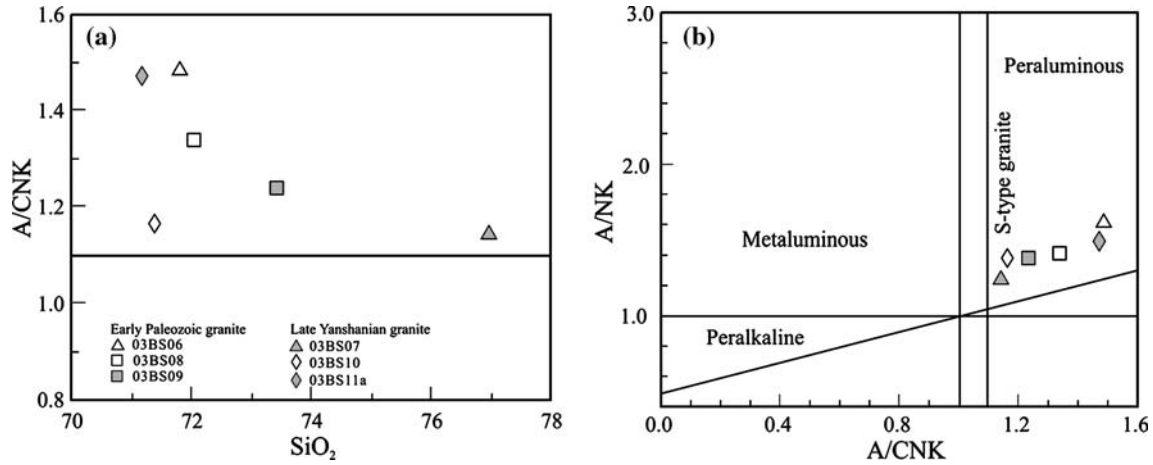

Fig. 2 SiO_2-content versus A/CNK ratio diagram (**a**) and A/CNK ratio versus A/NK ratio diagram (**b**) after Maniar and Piccoli (1989)

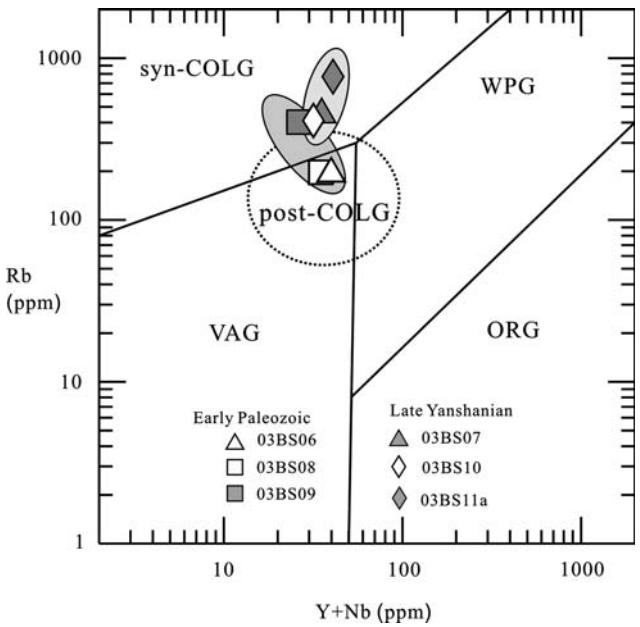

Fig. 3 Rb versus Y+Nb diagram after Pearce et al. (1984) and Pearce (1996). *ORG* ocean-ridge granitoid; *GPG* within-plate ganitoid; *VAG* volcanic granitoid; *COLG* collisional granitoid

the CL images (Fig. 6). Only one out of eight grains yielded nearly concordant U–Pb ages of about 80 Ma. Ages of inherited cores vary from late Proterozoic to early Paleozoic (upper intercepts at 828 ± 71 and 495 ± 150 Ma; Fig. 7c). Despite the lack of typical magmatic zoning and sponge-like CL textures, all the analyzed zircon grains from sample 03BS11a gave concordant or nearly concordant U–Pb ages, yielding a mean $^{206}Pb/^{238}U$ age of 60.9 ± 1.4 Ma (Fig. 7d).

A total of ninety-four zircon grains from the four granite samples were analyzed for Hf isotopic composition using the LA-MC-ICP MS method. Analytical data are given in Table 4. All analyzed zircon grains have low $^{176}Lu/^{177}Hf$ ratios, but measured $^{176}Hf/^{177}Hf$ ratios vary widely from 0.281816 to 0.282686 and corresponding $\varepsilon_{Hf}(0)$ values range from –33.8 to –3.0 but most data are between –16 and –10 (Table 4). The derived depleted-mantle modal ages $T_{DM}(Hf)$, calculated using a mean crustal Lu/Hf ratio ($^{176}Lu/^{177}Hf$ ratio of 0.015; Veevers et al. 2005), show a roughly similar distribution within the four samples. $T_{DM}(Hf)$ model ages range from 3,809 to 1,075 Ma (Fig. 8a–d), having a major peak at about 1,900 Ma and a minor peak of about 1,600 Ma (Fig. 8e). Combining all data, a mean $T_{DM}(Hf)$ model age of 1834 ± 46 Ma is obtained, which is close to whole rock $T_{DM}(Nd)$ model ages of the granites (Fig. 5). ε_{Hf} values of all the analyzed grains, calcaluted back to 470 Ma, range from about –37.9 to 7.1 (Fig. 8f), but most of the data cluster around –5. About 15% of analyzed grains have positive $\varepsilon_{Hf}(470\ Ma)$ values indicating that younger material (possibly of mantle origin) contributed to magma sources.

Discussion

Early Paleozoic magmatism

The Pingdajie granite, which intrudes the late Precambrian (?) to early Cambrian Gongyanghe Group, was previously dated at about 530–495 Ma by the Rb–Sr method and at 465–349 Ma by the K–Ar dating of mica. The granite is interpreted as a product of a Caledonian orogenic cycle (Yunnan Geological Survey 1981; Zhong 1998). Similar K–Ar mica ages of about 490 Ma have been obtained for other small granite bodies exposed in the Baoshan block (Yunnan Geological Survey 1981). Our study of single zircon U–Pb

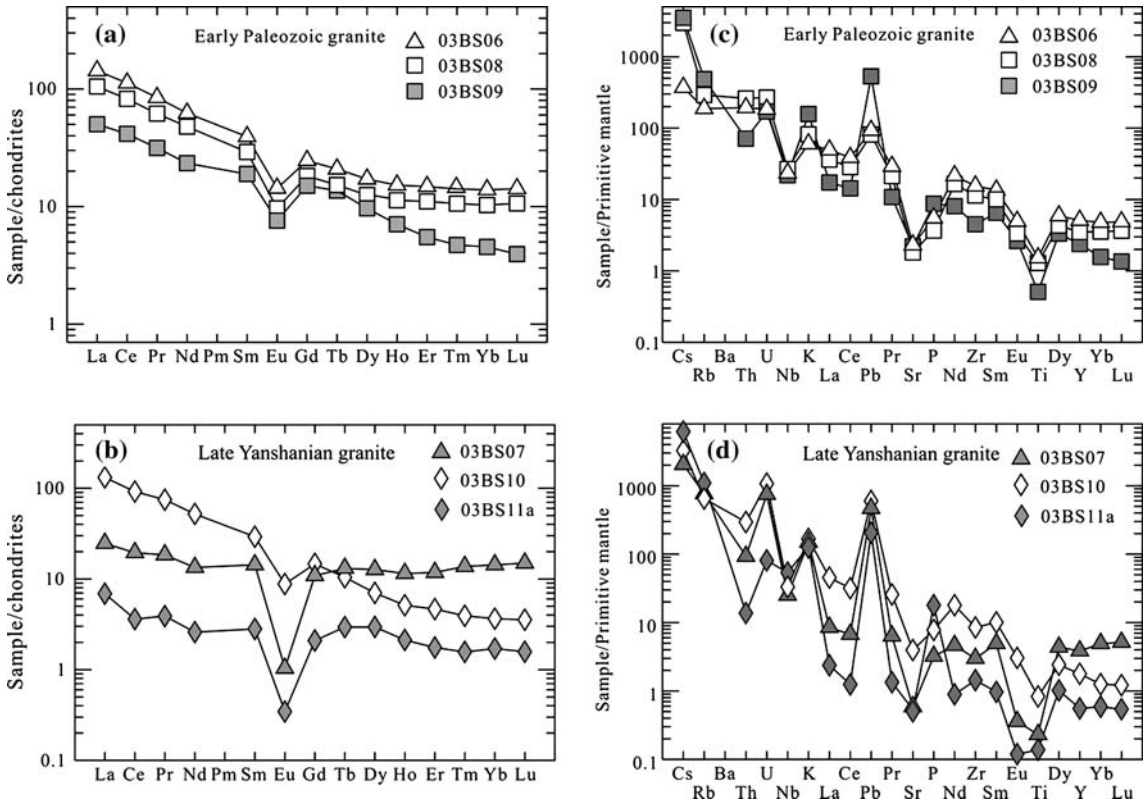

Fig. 4 Normalized REE and trace element content of the early Paleozoic Pingdajie granites (**a**, **c**) and the late Yanshanian Huataolin granites (**b**, **d**). Normalizing values for chondrite and primordial mantle are referred from Sun (1982) and Taylor and McLennan (1985)

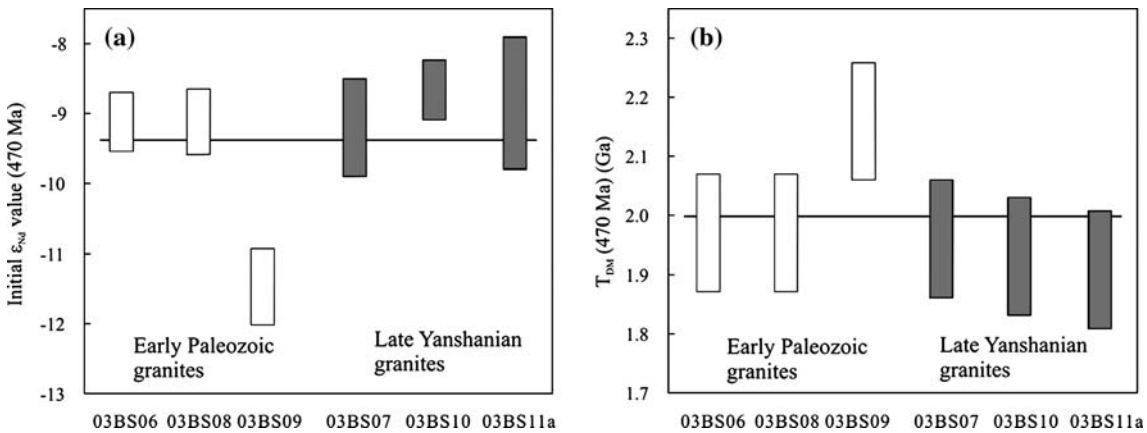

Fig. 5 **a** Initial ε_{Nd} values (calculated for an age of 470 Ma) and **b** depleted-mantle model ages T_{DM} for the early Paleozoic Pingdajie and the late Yanshanian Huataolin granites

dating yields an age of about 470 Ma for the crystallization time of the Pingdajie granite, providing a significantly more precise age than pre-exisiting age constraints. Contemporaneous magmatism was found in the eastern Sibumasu block, where a lens-shaped granite body in the late Paleozoic sedimentary sequence within the Nan-Uttaradit suture zone, the boundary between the Sibumasu and Indochina blocks, has been dated at 486 ± 5 Ma by the zircon U–Pb method (Metcalfe 1998). Early Paleozoic magmatism (e.g., the about 460 Ma old Dongpu granite) has been also found in the eastern Tibet (Li et al. 2002).

The tectonomagmatic evolution of the northern Gondwana margin is largely reflected in the presence of early Paleozoic orogenic and rift-related magmatic rocks (e.g., Matte 1986, 1991; Franke 1989; Pin 1990).

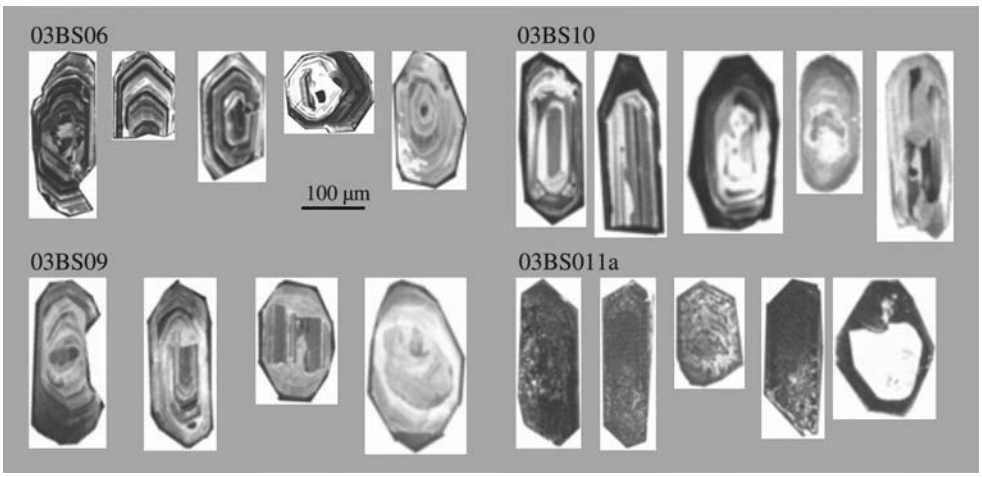

Fig. 6 Cathodoluminescence (*CL*) images of typical zircon populations for the early Paleozoic Pingdajie granite (03BS06, 03BS09) and the late Yanshanian Huataolin granite (03BS10, 03BS11a)

These magmatic associations can be traced in different tectono-metamorphic units of the European Variscides and the basement zones of the Alps (e.g., Oliver et al. 1993; Kröner and Hegner 1998; Von Quadt 1997; Dörr et al. 1998; Von Raumer 1998; Von Raumer et al. 2002 and references therein). According to palaeogeographic reconstructions the continental terranes of eastern and southeastern Asia rifted from India-NW Australian Gondwana margin (e.g., Metcalfe 1998, 2000, 2006). Early Paleozoic magmatism in the Baoshan block and in the neighboring regions implies a comparable history during the early Paleozoic between SE Asia and the western Tethyan region, e.g., the basement outcrops in the European Variscan belt, which are also considered as continental blocks having rifted from Gondwana prior to or simultaneously with those of SE Asia.

Late Yanshanian (Late Cretaceous to Early Tertiary) magmatism

The single zircon U–Pb dating results of sample 03BS10, collected from the Huataolin granite, demonstrate that inherited cores of late Proterozoic to early Paleozoic age are commonly present within these zircon grains. Low intercept model ages of 78 ± 4 and 76 ± 8 Ma obtained from two discordia lines provide age constraints for the formation of this granite. Zircon grains of sample 03BS11a give near concordant U–Pb ages around 61 Ma. Therefore, it is reasonable to suggest that the Huataolin granite formed between 78 and 61 Ma. Many contemporaneous granites can be found in the adjacent Tengchong block (Yunnan Geological Survey 1981). These magmatic rocks can be related to the closure of the Neotethys ocean. Mafic granulites found in the Yingjiang island-arc magmatic rocks on the border of Burma and in western Yunnan, west of the Tengchong block, were dated at about 74 Ma by the Ar–Ar laser-ablation technique and are interpreted as evidence for subduction of the Neotethys oceanic crust in southwestern Yunnan (Zhong et al. 1999).

Age and geochemical feature of the basement

The Tethyan belt in western Yunnan, or the Sanjiang area in Chinese literature, comprises several geological terranes of different origins. Information about the formation age and geochemical features of these terranes is essential for understanding the provenance and evolution of the Tethyan terranes in southwestern China. Both the early Paleozoic Pingdajie and the late Yanshanian Huataolin granites are peraluminous in composition and have low initial ε_{Nd} values at 470 Ma (–8.6 to –11.5), suggesting an origin by reworking of old crustal rocks that were situated beneath the Paleozoic sedimentary cover. Contribution of mantle material was probably of minor importance during the genesis of the early Paleozoic and late Yanshanian granitoids. Hence, inherited zircon ages, zircon Hf isotopic composition and whole rock Nd isotopic characteristics (initial ε_{Nd} values and Nd model ages) reflect charateristics of the basement rocks of the Baoshan block.

The close correspondance in geochemical and isotopic composition, especially in trace elements, whole rock Nd isotopic and zircon Hf isotopic composition, imply similar sedimentary protoliths for the early Paleozoic Pingdajie and the late Yanshanian Huataolin granites. Upper U–Pb intercept model ages suggest inherited zircon cores probably as old as early Archean in age (about 3.8 Ga; Fig. 7b). Whereas the early Paleozoic Pingdajie granite contains inherited zircons predominantly of Archean to Mesoproterozoic age, the late Yanshanian Huataolin granite bears evidence for

Table 3 Zircon U–Pb data of granites from the Baoshan block

Granite (sample)	$^{206}Pb/^{204}PB$	U (ppm)	Pb* (ppm)	Atomic ratios				Apparent ages (Ma)		
				$^{208}Pb^*/^{206}Pb^*$	$^{206}Pb^*/^{238}U$	$^{207}Pb^*/^{235}U$	$^{207}Pb^*/^{206}Pb^*$	$^{206}Pb^*/^{238}U$	$^{207}Pb^*/^{235}U$	$^{207}Pb^*/^{206}Pb^*$
Pingdajie granite (sample 03BS06)										
(1)	2,965	1,478	93.47	0.09	0.06400 ± 317	0.4938 ± 246	0.05595 ± 24	399.9	407.5	450.5
(2)	22,911	808	58.44	0.07	0.07464 ± 227	0.5818 ± 177	0.05653 ± 10	464.0	465.6	473.4
(3)	5,725	898	68.03	0.09	0.07655 ± 291	0.5980 ± 228	0.05666 ± 20	475.5	476.0	478.4
(4)	18,447	667	50.16	0.12	0.07449 ± 191	0.5810 ± 149	0.05656 ± 11	463.2	465.1	474.5
(5)	13,426	564	40.62	0.06	0.07506 ± 208	0.5870 ± 163	0.05672 ± 16	466.6	468.9	480.6
(6)	332	616	48.64	0.08	0.08061 ± 229	0.6413 ± 201	0.05770 ± 73	499.8	503.1	518.5
(7)	17,958	793	59.41	0.08	0.07681 ± 192	0.5994 ± 150	0.05660 ± 5	477.0	476.8	475.8
(8)	4,785	515	39.29	0.06	0.07939 ± 191	0.6223 ± 156	0.05685 ± 38	492.5	491.3	485.7
(9)	6,394	440	32.25	0.08	0.07509 ± 152	0.5913 ± 122	0.05711 ± 23	466.8	471.7	495.7
(10)	95	319	28.08	0.16	0.08298 ± 171	0.8564 ± 231	0.07485 ± 122	513.9	628.2	1064.6
(11)	907	529	40.69	0.11	0.07641 ± 155	0.6374 ± 130	0.06050 ± 13	474.6	500.7	621.5
(12)	2,485	661	50.28	0.08	0.07738 ± 157	0.6723 ± 172	0.06301 ± 99	480.5	522.1	708.6
(13)	992	550	39.67	0.03	0.07683 ± 158	0.6037 ± 126	0.05699 ± 16	477.2	479.6	491.2
Pingdajie granite (sample 03BS09)										
(1)	19,110	748	52.45	0.04	0.07428 ± 207	0.5790 ± 162	0.05633 ± 9	461.9	463.8	473.4
(2)	17,061	703	49.52	0.05	0.07413 ± 178	0.5805 ± 141	0.05680 ± 22	461.0	464.8	483.6
(3)	12,006	771	56.33	0.10	0.07352 ± 160	0.5789 ± 128	0.05711 ± 23	457.3	463.7	495.7
(4)	9,561	785	56.36	0.04	0.07572 ± 192	0.6101 ± 159	0.05844 ± 34	470.6	483.6	546.2
(5)	2,772	506	35.22	0.02	0.07494 ± 570	0.5832 ± 511	0.05644 ± 230	465.9	466.5	469.6
(6)	8,006	463	34.36	0.05	0.07824 ± 163	0.6216 ± 131	0.05762 ± 16	485.6	490.8	515.2
(7)	12,040	343	27.66	0.05	0.08466 ± 224	0.6843 ± 190	0.05863 ± 47	523.9	529.4	553.3
(8)	4,935	241	16.94	0.05	0.07345 ± 202	0.6242 ± 188	0.06164 ± 75	456.9	492.5	661.6
(9)	486	386	31.39	0.04	0.08599 ± 177	0.7465 ± 157	0.06296 ± 23	531.8	566.2	706.9
(10)	2,530	394	30.41	0.01	0.08391 ± 180	0.6553 ± 141	0.05664 ± 8	519.4	511.7	477.4
(11)	480	238	21.06	0.07	0.09035 ± 213	0.8977 ± 219	0.07206 ± 42	557.6	650.5	987.7
(12)	57	255	22.20	0.17	0.08088 ± 170	0.9225 ± 351	0.08272 ± 243	501.4	663.7	1262.6
Huataolin granite (sample 03BS10)										
(1)	5,139	1,382	20.70	0.05	0.01573 ± 39	0.1166 ± 33	0.05375 ± 14	100.6	112.0	360.7
(2)	14,852	997	24.59	0.06	0.02718 ± 64	0.1945 ± 46	0.05486 ± 14	163.7	180.5	406.7
(3)	9,122	1,410	18.94	0.03	0.01444 ± 56	0.0988 ± 39	0.04962 ± 33	92.4	95.7	177.3
(4)	6,380	1,334	19.93	0.06	0.01563 ± 52	0.1085 ± 37	0.05027 ± 45	100.1	104.6	207.3
(5)	6,708	1,133	12.87	0.15	0.02010 ± 58	0.1512 ± 44	0.05456 ± 29	128.3	143.0	394.0
(6)	785	1,222	14.37	0.05	0.01246 ± 47	0.0826 ± 34	0.04808 ± 72	79.8	80.6	103.3
(7)	1,662	691	16.88	0.08	0.02484 ± 80	0.1997 ± 74	0.05829 ± 103	158.2	184.8	540.8
(8)	4,833	1,069	17.01	0.05	0.01681 ± 36	0.1202 ± 27	0.05188 ± 30	107.4	115.3	280.2
Pingdajie granite (sample 03BS11a)										
(1)	625	1,942	16.12	0.01	0.00915 ± 25	0.0592 ± 30	0.04689 ± 197	58.7	58.4	43.7
(2)	420	1,331	12.22	0.00	0.01017 ± 30	0.0676 ± 21	0.04823 ± 34	65.2	66.4	110.7
(3)	352	1,464	12.81	0.03	0.00946 ± 21	0.0628 ± 17	0.04813 ± 69	60.7	61.8	105.9
(4)	394	1,511	13.52	0.03	0.00964 ± 26	0.0633 ± 18	0.04766 ± 47	61.8	62.4	82.6
(5)	255	1,146	9.69	0.02	0.00917 ± 28	0.0599 ± 29	0.04733 ± 171	58.9	59.0	66.1
(6)	407	1,265	10.69	0.03	0.00915 ± 21	0.0615 ± 18	0.04879 ± 87	58.7	60.6	147.6
(7)	192	741	6.59	0.02	0.00967 ± 25	0.0668 ± 19	0.05020 ± 58	61.9	65.6	204.2
(8)	185	889	7.92	0.01	0.00977 ± 21	0.0635 ± 18	0.04718 ± 91	62.7	62.6	58.2
(9)	260	964	8.23	0.01	0.00934 ± 35	0.0632 ± 25	0.04906 ± 52	59.9	62.2	150.8
(10)	249	771	6.66	0.01	0.00954 ± 21	0.0612 ± 18	0.04648 ± 83	61.2	60.3	22.9

Concentrations were calculated using estimated zircon weights Standard errors on the isotopic ratios are given at the 95% confidence level in the last digit place. Values of $^{206}Pb/^{204}Pb$ ratios are measured values. Measured data were calculated using the ''Pbdat'' program (Ludwig 1988)

Neoproterozoic to early Paleozoic inherited zircon cores. Nd model ages (T_{DM}) of the granites clustering around 2.0 Ga indicate an avearge late Paleoproterozoic crustal residence time for the precursor rocks. These model ages are generally older compared to those from basement rocks exposed in the European Variscides (Liew and Hofmann 1988; Hegner and Kröner 2000). A histogram of T_{DM}(Hf) values of the four analysed samples (Fig. 8e) shows two peak values around 1.9–1.8 and 1.6–1.4 Ga. Some zircon grains give

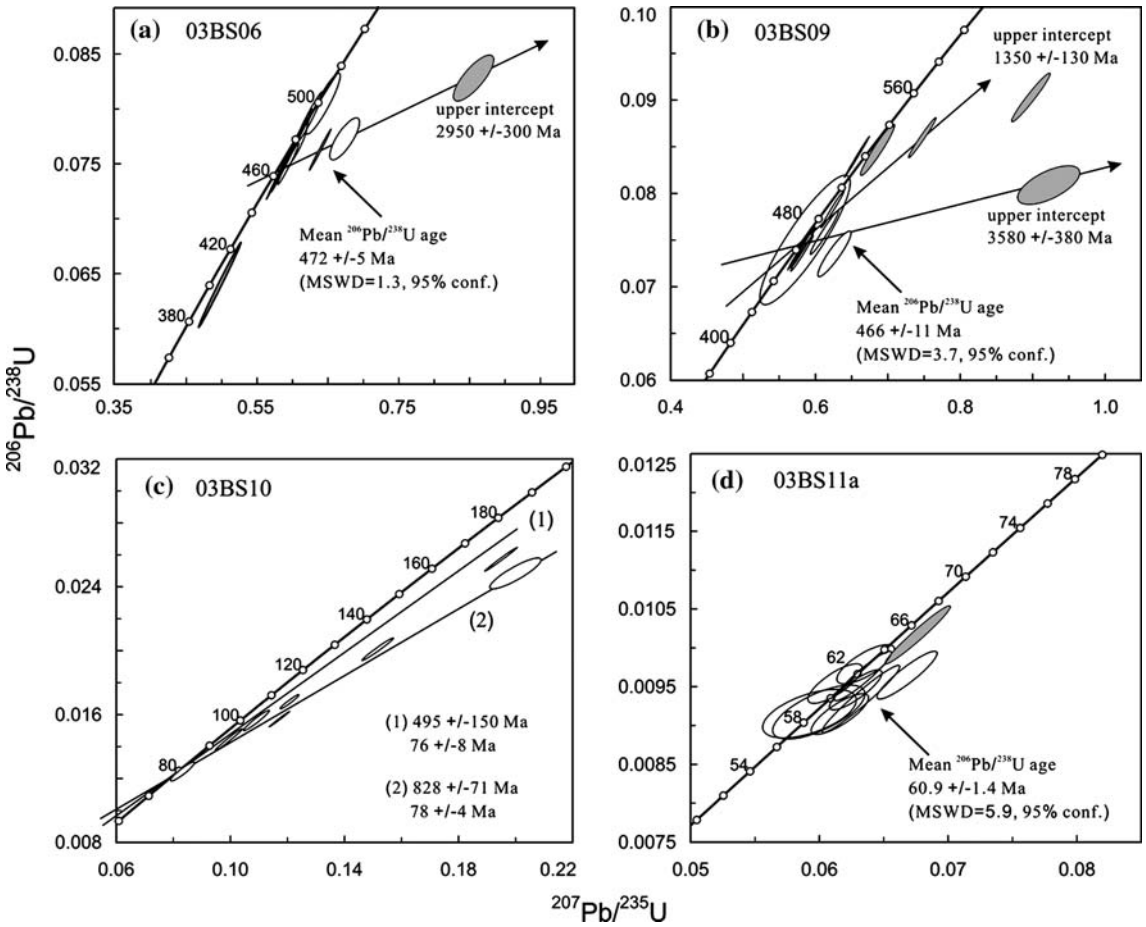

Fig. 7 Zircon U-Pb concordia diagrams for the early Paleozoic Pingdajie granite (**a**, **b**) and the late Yanshanian Huataolin granites (**c**, **d**)

Archean T_{DM}(Hf) values between 3.8–2.6 Ga. Geochemical data indicate S-type characteristic for both the Pingdajie and Huataolin granites. In general, great care must be taken to insure that model ages which only rely on one isotope system, e.g., Sm–Nd, are not misinterpreted with respect to crustal residence times and source ages. This holds true in particular for the evaluation of S-type anatectic magmas (Clemens 2003), which can be derived from a number of crustal sources of different age. In the present study we have combined U–Pb data from inherited zircon ages and Nd–Hf isotopic data to put constraints on the crustal residence time of the two granites from the Baoshan block. The data imply that magma sources of the granites are likely made up mainly of Paleoproterozoic to Mesoproterozoic crustal material. Some zircon grains from both the early Paleozoic Pingdajie and late Yanshanian Huataolin granites have positive initial ε_{Hf} values at 470 Ma, i.e., the formation age of the early Paleozoic granite. This implies that the addition of juvenile (or newly mantle derived) material to the crust played some role, at least during the formation of the Pingdajie granite. However, the proportion of material sources of different ages is difficult to estimate. As mentioned above, continental terranes of E and SE Asia probably originated from the India-N/NW Australian margin of the Gondwana supercontinent (e.g., Metcalfe 1998, 2000, 2006), where Archean to Paleoproterozoic cratonic blocks are exposed (e.g., Barley 1997; Myers and Swagers 1997; van Kranendonk and Collins 1998; Wingate and Evans 2003; Yedekar et al. 1990; Jain et al. 1991; Mazumder et al. 2000; Dobmeier and Raith 2003). These cratons could have served as a major source region during the formation of the Baoshan basement. Inherited zircon ages and Nd-Hf isotopic composition of the early Paleozoic and late Yanshanian granites bear evidence for an India-N/NW Australian origin for the underlying basement of the Baoshan block. The detrital zircons of Archean age were probably derived from Archean terranes in India (e.g., the Singhbhum and Bastar cratons) or western Australia (e.g., the Yilgarn and Pilbara cratons), whereas the zircons of Paleoproterozoic age could have been derived from similar terranes in NW Australia.

Table 4 Zircon Hf isotopic composition of granites from the Baoshan block

Zircon No.	$^{176}Lu/^{177}Hf$	$^{176}Hf/^{177}Hf$	$2\sigma_m$	$\varepsilon Hf(0)$	$\varepsilon Hf(t)$ 470 Ma	$\varepsilon Hf(t)$ 65 Ma	T_{DM} C	$f_{Lu/Hf}$
Pingdajie granite (sample 03BS06, 470 Ma)								
1	0.00147	0.282319	0.000117	–16.0	–6.1		1,845	–0.96
2	0.00138	0.282173	0.000123	–21.2	–11.3		2,168	–0.96
3	0.00262	0.282350	0.000079	–14.9	–5.4		1,799	–0.92
4	0.00413	0.282455	0.000079	–11.2	–2.2		1,594	–0.88
5	0.00245	0.282326	0.000065	–15.8	–6.2		1,848	–0.93
6	0.00092	0.282363	0.000067	–14.5	–4.4		1,735	–0.97
7	0.00109	0.282313	0.000070	–16.2	–6.2		1,851	–0.97
8	0.00302	0.282467	0.000071	–10.8	–1.4		1,544	–0.91
9	0.00141	0.282281	0.000043	–17.4	–7.5		1,928	–0.96
10	0.00152	0.282342	0.000020	–15.2	–5.3		1,794	–0.95
11	0.00300	0.282342	0.000018	–15.2	–5.8		1,825	–0.91
12	0.00105	0.282304	0.000054	–16.6	–6.6		1,871	–0.97
13	0.00382	0.282304	0.000049	–16.6	–7.4		1,926	–0.88
14	0.00219	0.282322	0.000075	–15.9	–6.3		1,853	–0.93
15	0.00113	0.282301	0.000075	–16.7	–6.7		1,879	–0.97
16	0.00347	0.282374	0.000086	–14.1	–4.8		1,761	–0.90
17	0.00112	0.282307	0.000049	–16.4	–6.4		1,864	–0.97
18	0.00684	0.282565	0.000065	–7.3	0.9		1,400	–0.79
19	0.00123	0.282334	0.000057	–15.5	–5.5		1,807	–0.96
20	0.00108	0.282308	0.000045	–16.4	–6.4		1,861	–0.97
21	0.00067	0.282224	0.000094	–19.4	–9.3		2,041	–0.98
22	0.00131	0.282372	0.000053	–14.1	–4.2		1,722	–0.96
Pingdajie granite (sample 03BS09, 470 Ma)								
1	0.00134	0.282203	0.000049	–20.1	–10.2		2,100	–0.96
2	0.00203	0.282295	0.000051	–16.9	–7.2		1,909	–0.94
3	0.00333	0.282321	0.000044	–15.9	–6.7		1,877	–0.90
4	0.00123	0.282345	0.000060	–15.1	–5.2		1,783	–0.96
5	0.00102	0.282180	0.000052	–20.9	–10.9		2,146	–0.97
6	0.00150	0.282214	0.000059	–19.7	–9.9		2,079	–0.95
7	0.00011	0.282199	0.000045	–20.3	–10.0		2,086	–1.00
8	0.00064	0.281792	0.000055	–34.7	–24.5		2,993	–0.98
9	0.00100	0.282199	0.000052	–20.3	–10.2		2,103	–0.97
10	0.00195	0.282665	0.000066	–3.8	6.0		1,075	–0.94
11	0.00140	0.282250	0.000059	–18.5	–8.6		1,998	–0.96
12	0.00124	0.282505	0.000034	–9.4	0.5		1,424	–0.96
13	0.00140	0.282114	0.000044	–23.3	–13.4		2,301	–0.96
14	0.00208	0.282271	0.000140	–17.7	–8.0		1,963	–0.94
15	0.00105	0.282143	0.000052	–22.3	–12.3		2,230	–0.97
16	0.00100	0.281419	0.000036	–47.8	–37.9		3,809	–0.97
17	0.00144	0.282327	0.000049	–15.8	–5.9		1,828	–0.96
18	0.00147	0.282393	0.000109	–13.4	–3.5		1,680	–0.96
19	0.00160	0.282459	0.000032	–11.1	–1.2		1,533	–0.95
20	0.00136	0.282541	0.000042	–8.2	1.8		1,344	–0.96
Huataolin granite (sample 03BS10, 78 Ma)								
1	0.00134	0.282024	0.000027	–26.4	–16.5	–25.1	2,691	–0.96
2	0.00150	0.282415	0.000027	–12.6	–2.8	–11.3	1,832	–0.95
3	0.00284	0.282549	0.000022	–7.9	1.6	–6.6	1,540	–0.91
4	0.00083	0.282548	0.000023	–7.9	2.1	–6.5	1,534	–0.98
5	0.00087	0.282537	0.000014	–8.3	1.8	–6.9	1,557	–0.97
6	0.00061	0.282425	0.000011	–12.3	–2.1	–10.9	1,805	–0.98
7	0.00209	0.282394	0.000014	–13.4	–3.7	–12.1	1,882	–0.94
8	0.00071	0.282580	0.000017	–6.8	3.3	–5.4	1,461	–0.98
9	0.00027	0.282508	0.000011	–9.3	0.9	–7.9	1,620	–0.99
10	0.00071	0.282595	0.000018	–6.3	3.8	–4.9	1,429	–0.98
11	0.00108	0.281816	0.000020	–33.8	–23.8	–32.4	3,143	–0.97
12	0.00151	0.282416	0.000016	–12.6	–2.7	–11.2	1,813	–0.95
13	0.00071	0.282619	0.000015	–5.4	4.7	–4.0	1,374	–0.98
14	0.00033	0.282423	0.000015	–12.3	–2.1	–10.9	1,809	–0.99
15	0.00115	0.282366	0.000014	–14.4	–4.4	–13.0	1,940	–0.97
16	0.00085	0.282563	0.000018	–7.4	2.7	–6.0	1,501	–0.97

Table 4 continued

Zircon No.	$^{176}Lu/^{177}Hf$	$^{176}Hf/^{177}Hf$	$2\sigma_m$	$\varepsilon Hf(0)$	$\varepsilon Hf(t)$ 470 Ma	$\varepsilon Hf(t)$ 65 Ma	T_{DM} C	$f_{Lu/Hf}$
17	0.00133	0.282412	0.000016	–12.7	–2.8	–11.4	1,837	–0.96
18	0.00003	0.282429	0.000014	–12.1	–1.8	–10.7	1,794	–1.00
19	0.00037	0.282572	0.000016	–7.1	3.2	–5.7	1,477	–0.99
20	0.00073	0.282313	0.000014	–16.2	–6.1	–14.8	2,054	–0.98
21	0.00078	0.282520	0.000018	–8.9	1.2	–7.5	1,595	–0.98
22	0.00057	0.282686	0.000013	–3.0	7.1	–1.6	1,223	–0.98
23	0.00134	0.282387	0.000016	–13.6	–3.7	–12.3	1,893	–0.96
Huataolin granite (sample 03BS11a, 61 Ma)								
1	0.00462	0.282373	0.000010	–14.1	–5.2	–12.9	1,937	–0.86
2	0.00381	0.282380	0.000011	–13.9	–4.7	–12.6	1,918	–0.89
3	0.00091	0.282601	0.000013	–6.0	4.0	–4.6	1,414	–0.97
4	0.00627	0.282384	0.000014	–13.7	–5.4	–12.6	1,921	–0.81
5	0.00468	0.282335	0.000010	–15.4	–6.6	–14.2	2,022	–0.86
6	0.00292	0.282391	0.000009	–13.5	–4.0	–12.2	1,891	–0.91
7	0.00266	0.282362	0.000012	–14.5	–5.0	–13.2	1,954	–0.92
8	0.00184	0.282371	0.000010	–14.2	–4.4	–12.8	1,930	–0.94
9	0.00520	0.282333	0.000015	–15.5	–6.8	–14.3	2,028	–0.84
10	0.00333	0.282371	0.000010	–14.2	–4.9	–12.9	1,938	–0.90
11	0.00543	0.282377	0.000016	–14.0	–5.3	–12.8	1,933	–0.84
12	0.00041	0.282403	0.000017	–13.0	–2.8	–11.6	1,854	–0.99
13	0.00422	0.282353	0.000012	–14.8	–5.8	–13.6	1,980	–0.87
14	0.00203	0.282419	0.000016	–12.5	–2.8	–11.2	1,826	–0.94
15	0.00147	0.282144	0.000013	–22.2	–12.3	–20.8	2,429	–0.96
16	0.00344	0.282363	0.000011	–14.5	–5.2	–13.2	1,956	–0.90
17	0.00359	0.282361	0.000010	–14.5	–5.3	–13.3	1,960	–0.89
18	0.00099	0.282526	0.000015	–8.7	1.3	–7.3	1,583	–0.97
19	0.00458	0.282365	0.000009	–14.4	–5.5	–13.2	1,954	–0.86
20	0.00323	0.282405	0.000008	–13.0	–3.7	–11.7	1,862	–0.90
21	0.00243	0.282540	0.000015	–8.2	1.4	–6.9	1,558	–0.93
22	0.00460	0.282376	0.000013	–14.0	–5.1	–12.8	1,931	–0.86
23	0.00077	0.282070	0.000013	–24.8	–14.7	–23.4	2,588	–0.98
24	0.00120	0.282269	0.000014	–17.8	–7.8	–16.4	2,153	–0.96
25	0.00223	0.282401	0.000009	–13.1	–3.5	–11.8	1,865	–0.93
26	0.00390	0.282380	0.000010	–13.9	–4.7	–12.6	1,919	–0.88
27	0.00421	0.282366	0.000011	–14.4	–5.4	–13.1	1,953	–0.87
28	0.00157	0.282382	0.000009	–13.8	–4.0	–12.4	1,906	–0.95
29	0.00330	0.282373	0.000008	–14.1	–4.8	–12.8	1,933	–0.90

T_{DM}C values are calculated by using a mean $^{176}Lu/^{177}Hf$ value of 0.015 for crustal material

Conclusions

Granites intruding the Gongyanghe Group in the Baoshan block of the Tethyan Yunnan can be devided into two groups whose emplacement is dated at about 470 Ma (Pingdajie granite) and about 78–61 Ma (late Yanshanian Huataolin granite). Geochemical and isotopic characteristics indicate that both granites mainly originated from intra-crustal reworking during two different tectonic events. The late Yanshanian magmatism is probably related to the closure of the Neotethys ocean. The early Paleozoic magmatism is more or less contemporaneous with magmatism in the neighboring areas of SE Asia (e.g., the eastern Sibumasu block and the eastern Tibet) and in the western Tethyan belt (e.g. the inner-Alpine belt and European Variscides), supporting a common derivation and separation of the different crystalline units from northern margins of Gondwana during the early Paleozoic.

Contents of trace elements in the early Paleozoic Pingdajie granite are very similar to contents found in the late Yanshanian Huataolin granite. The same holds true for the Nd–Hf isotopic record. It is concluded that both granites were derived from a similar magma sources that represent a record of the Tethyan Yunnan basement. The early Paleozoic granite contains early Archean to Mesoproterozoic inherited zircon cores, whereas the late Yanshanian granite contains late Proterozoic to early Paleozoic inherited zircons. Nd–Hf isotopic data of the granites imply Paleoproterozoic to Mesoproterozoic crustal material as the major components of the underlying basement. It is proposed that the basement was derived from the Archean and Paleoproterozoic terrains in India and NW Australia. This conclusion is consistent with a Gondwana origin

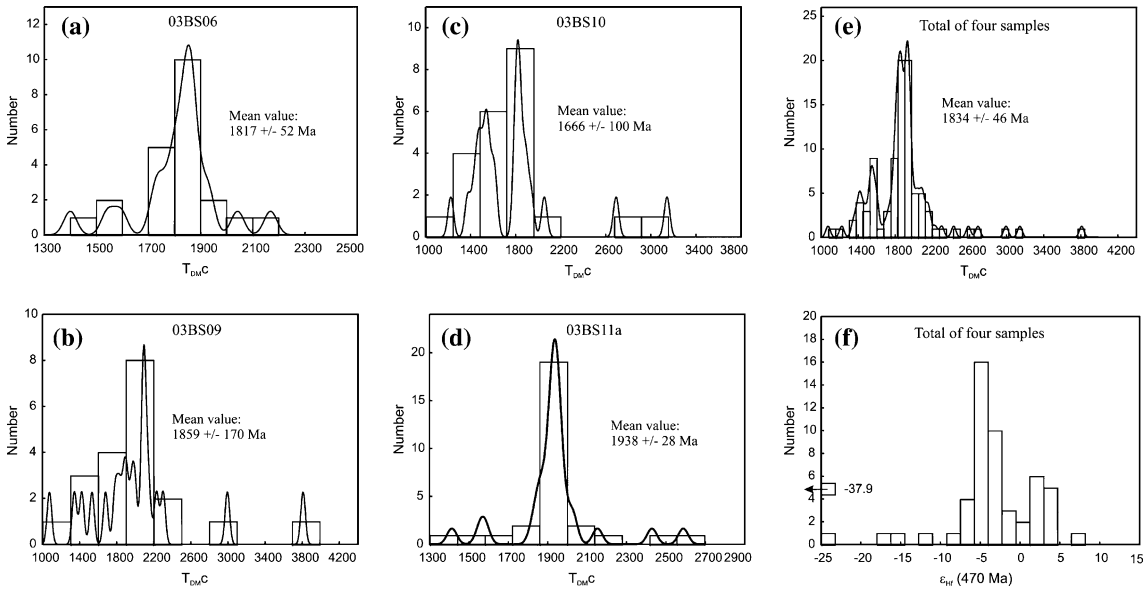

Fig. 8 Zircon Hf isotopic composition of granite samples. **a–d** histograms of T_{DM}(Hf) values of zircon samples from the early Paleozoic Pingdajie granite (03BS06 and 03BS09) and the late Yanshanian Huataolin granite (03BS10 and 03BS11a); **e** histograms of T_{DM}(Hf) values of zircon grains from the four granite samples, mostly clustering around 1,800 Ma. **f** histogram of initial ε_{Hf} values (470 Ma) of zircon grains from four granite samples, mostly clustering around –4

of the continental terrains in SE Asia, which was previously proposed on the basis of tectono-stratigraphic, palaeontological and geophysical data (Metcalfe 1998).

Acknowledgements This study was supported by the National Natural Science Foundation of China (NSFC project Nos. 40372106, 40525007 and 40421202). Metcalfe I. and Koralay E. are gratefully acknowleged for constructive comments to improve the manuscript. Sincere thanks are given to Liu Yan for help during field work, Ma Yuguan and Xie Liewen for assistance with zircon CL and Hf isotope analyses.

References

Barley ME (1997) The Pilbara Craton. In: De Wit MJ, Ashwal LD (eds) Greenstone belts. Clarendon, Oxford, pp 657–663

Blichert-Toft J, Albarede F (1997) The Lu–Hf geochemistry of chondrites and evolution of the mantle-crust system. Earth Planet Sci Lett 148:243–258

Chen F, Hegner E, Todt W (2000) Zircon ages and Nd isotopic and chemical compositions of orthogneisses from the Black Forest, Germany: evidence for a Cambrian magmatic arc. Int J Earth Sci 88:791–802

Chen F, Satir M, Ji J-Q, Zhong D-L (2002a) Nd–Sr–Pb isotopic composition of the Cenozoic volcanic rocks from western Yunnan, China: evidence for enriched mantle source. J Asian Earth Sci 21:39–45

Chen F, Siebel W, Satir M (2002b) Zircon U–Pb and Pb-isotope fractionation during stepwise HF-acid leaching and chronological implications. Chem Geol 191:155–164

Chen F, Siebel W, Satir M, Terzioglu N, Saka K (2002c) Geochronology of the Karadere basement (NW Turkey) and implications for the geological evolution of the Istanbul zone. Int J Earth Sci 91:469–481

Chu N-C, Taylor RN, Chavagnac V, Nesbitt RW, Boella RM, Milton JA, German C, Bayon G, Burton M (2002) Hf isotope ratio analysis using multi-collector inductively coupled plasma mass spectrometry: an evaluation of isobaric interference corrections. J Anal Atom Spectr 17:1567–1574

Clemens JD (2003) S-type granitic magmas—petrogenetic issues, models and evidence. Earth Sci Rev 61:1–18

Dobmeier CJ, Raith MM (2003) Crustal architecture and evolution of the Eastern Ghats Belt and adjacent regions of India. In: Yoshida M, Windley BF, Dasgupta S (eds) Proterozoic East Gondwana: supercontinent assembly and breakup. Geol Soc Lond, Spec Publ 206:145–168

Dörr W, Fiala J, Vejnar Z, Zulauf G (1998) U-Pb zircon ages and structural development of metagranitoids of the Tepla crystalline complex: evidence for pervasive Cambrian plutonism within the Bohemian massif (Czech Republic). Geol Rundsch 87:135–149

Fan P-F (1978) Outline of the tectonic evolution of southwestern China. Tectonophysics 45:261–267

Franke W (1989) Tectonostratigraphic units in the Variscan belt of central Europe. Geol Soc Am Spec Paper 230:67–90

Gansser A (1981) The geodynamic history of the Himalaya. In: Gupta HK, Delany FM (eds) Zagros-Hindukush-Himalaya: geodynamic evolution. American Geophysical Union, pp 11–21

Griffin WL, Pearson NJ, Belousova E, Jackson SE, van Achterbergh E, O'Reilly SY, Shee SR (2000) The Hf isotope composition of cratonic mantle: LAM-MC-ICPMS analysis of zircon megacrysts in kimberlites. Geochim Cosmochim Acta 64:133–147

Hanchar JM, Miller CF (1993) Zircon zonation patterns as revealed by cathodoluminescence and backscattered electron images: implications for interpretation of complex crustal histories. Chem Geol 110:1–13

Hegner E, Kröner A (2000) Review of Nd isotopic data and xenocrystic and detrital zircon ages from the pre-Variscan basement in the eastern Bohemian Massif: speculations on

palinspastic reconstructions. In: Franke W, Haak V, Oncken O, Tanner D (eds) Orogenic processes: quantification and modeling in the Variscan belt. Geol Soc Lond Spec Publ 179:113–129

Hutchison CS (1993) Gondwana and Cathaysian blocks, Palaeotethys sutures and Cenozoic tectonics in South-east Asia. Geol Rundsch 82:388–405

Jain SC, Yedekar DB, Nair KKK (1991) Central India shear zone: a major Precambrian crustal boundary. J Geol Soc India 37:521–531

Jin X-C (2002) Permo-Carboniferous sequences of Gondwana affinity in southwest China and their paleographic implications. J Asian Earth Sci 20:633–646

Krogh TE (1982) Improved accuracy of U-Pb zircon ages by the creation of more concordant systems using an air abrasion technique. Geochim Cosmochim Acta 46:637–649

Kröner A, Hegner E (1998) Geochemistry, single zircon ages and Sm–Nd systematics of granitoid rocks from the Gory Sowie (Owl Mts), Polish West Sudetes; evidence for early Palaeozoic arc-related plutonism. J Geol Soc Lond 155:711–724

Kröner A, Jaeckel P, Reischmann T, Kroner U (2001) Single zircon ages and whole-rock Nd isotopic systematics of early Palaeozoic granitoid gneisses from the Czech and Polish Sudetes (Jizerske Hory, Krkonose Mountains and Orlice–Sneznik Complex). Int J Earth Sci 90:304–324

Li X-Z, Jiang X-S, Sun Z-M, Shen G-F, Du D-X (2002) The collisional orogenic processes of the Nujiang–Lancangjiang–Jinshajiang area, southwestern China. Geological Press House, Beijing, pp 1–213

Liew TC, Hofmann AW (1988) Precambrian crustal components, plutonic associations, plate environment of the Hercynian Fold Belt of central Europe: indications from a Nd and Sr isotopic study. Contrib Mineral Petrol 98:129–138

Ludwig KR (1988) Pbdat for MS-Dos—a computer program for IBM-PC compatibles for processing raw Pb–U–Th isotope data. US Geol Surv, Open-file Rep 88–542:1–37

Ludwig KR (2001) Isoplot/Ex, rev 2.49: a geochronological toolkit for Microsoft Excel. Berkeley Geochron. Center Spec Publ No. 1a:1–58

Machado N, Simonetti A (2001) U–Pb dating and Hf isotopic composition of zircon by laser ablation MC-ICP-MS, In: Sylvester P (ed) Laser ablation-ICPMS in the earth sciences: principles and applications. St John's, Newfoundland, Mineral Assoc Canada 29:121–146

Maniar PD, Piccoli PM (1989) Tectonic discrimination of granitoids. Bull Am Geol Soc 101:635–643

Matte P (1986) Tectonics and plate tectonics model for the Variscan belt of Europe. Tectonophysics 126:329–374

Matte P (1991) Accretionary history and crustal evolution of the Variscan belt in Western Europe. Tectonophysics 196:309–337

Mazumder R, Bose PK, Sarkar S (2000) A commentary on the tectono-sedimentary records of the pre-2.0 Ga continental growth of India vis-à-vis a possible pre-Gondwana Afro-Indian super-continent. J Asian Earth Sci 30:201–217

Metcalfe I (1988) Origin and assembly of Southeast Asian continental terranes. In: Audley-Charles MG, Hallam A (eds) Gondwana and Tethys. Geol Soc Lond, Spec Publ 37:101–118

Metcalfe I (1996a) Pre-Cretaceous evolution of SE Asian terranes. In: Hall R, Blundell D (eds) Tectonic evolution of Southeast Asia. Geol Soc Spec Publ 106:97–122

Metcalfe I (1996b) Gondwanaland dispersion, Asian accretion and evolution of eastern Tethys. Austr J Earth Sci 43:605–623

Metcalfe I (1998) Palaeozoic and Mesozoic geological evolution of the SE Asian region, multidisciplinary constraints and implications for biogeography. In: Hall R, Holloway JD (eds) Biogeography and geological evolution of SE Asia. Backhuys Publishers, Amsterdam, pp 25–41

Metcalfe I (2002) Permian tectonic framework and palaeogeography of SE Asia. J Asian Earth Sci 20:551–566

Metcalfe I (2006) Palaeozoic and Mesozic tectonic evolution and palaeogeography of East Asian crustal fragmets: the Korean Peninsula inI context. Gondwana Res 9:24–46

Myers JS, Swagers C (1997) The Yilgarn Craton. In: De Wit MJ, Ashwal LD (eds) Greenstone belts. Clarendon, Oxford, pp 640–656

Neumayr M (1885) Die geographische Verbreitung der Juraformation. Denkschr Kais Koenig Akad Wiss Wien, math-nat Cl 15:57–114

Oliver GJH, Corfu F, Krogh TE (1993) U-Pb ages from SW poland, evidence for a Caledonia structure zone between Baltica and Gondwana. J Geol Soc Lond 150:355–369

Parrish RR (1987) An improved micro-capsule for zircon dissolution in U–Pb geochronology. Chem Geol 66:99–102

Pearce JA (1996) Sources and settings of granitic rocks. Episode 19:120–125

Pearce JA, Harris NB, Tindle AG (1984) Trace element discrimination diagrams for the tectonic interpretation of granitic rocks. J Petrol 25:956–983

Pidgeon RT, Nemchin AA, Hitchen GJ (1998) Internal structures of zircons from Archaean granites from the Darling Range Batholith; implications for zircon stability and the interpretation of zircon U–Pb ages. Contrib Mineral Petrol 132:288–299

Pin C (1990) Variscan oceans—ages, origins and geodynamic implications inferred from geochemical and radiometric data. Tectonophysics 177:215–227

Poller U, Liebetrau V, Todt W (1997) U–Pb single-zircon dating under cathodoluminescence control (CLC-method): application to polymetamorphic orthogneisses. Chem Geol 139:287–297

Powell CMcA, Johnson BD (1980) Constraints on the Cenozoic position of Sundaland. Tectonophysics 63:91–109

von Quadt A (1997) U–Pb zircon and Sr–Nd–Pb whole-rock investigations from the continental deep drilling (KTB). Geol Rundsch 86(supp l):258–271

von Raumer JF (1998) The Palaeozoic evolution in the Alps: from Gondwana to Pangea. Geol Rundsch 87:407–435

von Raumer JF, Stampfli GM, Borel G, Bussy F (2002) Reorganization of pre-Variscan basement areas at the north-Gondwanan margin. Int J Earth Sci 91:35–52

Rowley DB (1996) Age of initiation of collision between India and Asia: a review of stratigraphic data. Earth Planet Sci Lett 145:1–13

Sengör AMC, Natal'in BA (1996) Palaeotectonics of Asia, fragments of a synthesis. In: Yin A, Harrison TM (eds) Tectonic evolution of Asia. Cambridge University Press, Cambridge, pp 486–640

Sengör AMC, Altiner D, Cin A, Ustaomer T, Hsü KJ (1988) Origin and assembly of the Tethyside orogenic collage at the expense of Gondwana Land. In: Audley-Charles MG, Hallam A (Eds. Gondwana and Tethys. Geol Soc Spec Publ 37:119–181

Shi G-R, Archbold NW (1995) Permian brachiopod faunal sequence of the Shan-Thai terrane: biostratigraphy, palaeobiogeographical affinities and plate tectonic/palaeoclimatic implications. J SE Asian Earth Sci 11:177–187

Shi G-R, Archbold NW (1998) Permian marine biogeography of SE Asia. In: Hall R, Holloway JD (eds) Biogeography and geological evolution of SE Asia. Backhuys Publishers, Amsterdam, pp 57–72

Stacey JS, Kramers JD (1975) Approximation of terrestrial lead isotope evolution by a two stage model. Earth Planet Sci Lett 127:30–45

Suess E (1893) Are great oceans depths permanent? Nat Sci 2:180–187

Sun SS (1982) Chemical composition and origin of the Earth's primitive mantle. Geochim Cosmochim Acta 46:179–192

Tapponier P, Mercier JL, Proust F, Andrieux J, Armijo R, Bassoullet JP, Burnel M, Burg JP, Colchen M, Dupre B, Girardeau J, Marcoux J, Mascle G, Matte P, Nicolas A, Li TD (1981) The Tibetan side of the India-Eurasia collision. Nature 294:405–410

Taylor SR, McLennan SM (1985) The continental crust: its composition and evolution. Blackwell, Oxford, pp 1–312

Ueno K (2000) Permian fusulinacean faunas of the Sibumasu and Baoshan blocks, implications for the paleogeographic reconstruction of the Cimmerian continent. Geosci J 4:160–163

Van Kranendonk MJ, Collins WJ (1998) Timing and tectonic significance of Late Archaean, sinistral strike-slip deformation in the Central Pilbara Structural Corridor, Pilbara Craton, Western Australia. Precamb Res 88:207–232

Veevers JJ, Saeed A, Belousova EA, Griffin WL (2005) U–Pb ages and source composition by Hf-isotope and trace-element analysis of detrital zircons in Permian sandstone and modern sand from southwestern Australia and a review of the paleogeographical and denudational history of the Yilgarn Craton. Earth Sci Rev 68:245–279

Wang X-D, Ueno K, Mizuno Y, Sugiyama T (2001) Late Paleozoic faunal, climatic, and geographic changes in the Baoshan Block as a Gondwana-derived continental fragment in southwest China. Palaeogeogr Palaeoclimat Palaeoecol 170:197–218

Wiedenbeck M, Allé P, Corfu F, Griffin WL, Meier M, Oberli F, Von Quadt A, Roddick JC, Spiegel W (1995) Three natural zircon standards for U–Th–Pb, Lu–Hf, trace element and REE analyses. Geostand Newslett 19:1–23

Wingate MTD, Evans DAD (2003) Palaeomagnetic constraints on the Proterozoic tectonic evolution of Australia. In: Yoshida M, Windley BF, Dasgupta S (eds) Proterozoic East Gondwana: supercontinent assembly and breakup. Geol Soc Lond Spec Publ 206:77–91

Woodhead J, Hergt J, Shelley M, Eggins S, Kemp R (2004) Zircon Hf-isotope analysis with an excimer laser, depth profiling, ablation of complex geometries, and concomitant age estimation. Chem Geol 209: 121–135

Wopfner H (1996) Gondwana origin of the Baoshan and Tengchong terrenes of west Yunnan. In: Hall R, Blundell D (eds) Tectonic evolution of Southeast Asia. Geol Soc Spec Publ 106:539–547

Wu H, Boulter CA, Ke B, Stow DAV, Wang Z (1995) The Changning-Menglian suture zone; a segment of the major Cathaysian-Gondwana divide in Southeast Asia. Tectonophysics 242:267–280

Xu P, Wu F-Y, Xie L-W, Yang Y-H (2004) Hf isotopic composition of the standard zircons for the U–Pb dating. Chin Bull Sci 49:1042–1410

Yedekar DB, Jain SC, Nair KKK (1990) The central Indian collision suture, Precambrian central India. Geol Soc India, Spec Publ 28:1–27

Yunnan Geological Survey (1981) Guidebook for geological map of Yunnan Province (1: 500 000). pp 1–122

Zhong D-L (1998) Paleo-Tethyan orogenic belt in the western parts of the Sichuan and Yunnan Provinces. Science Press, Beijing, pp 231

Zhong D-L, Ji J-Q, Hu S-L (1999) Subduction age of Neo-Tethys oceanic crust in Southwest Yunnan, China: laser micro-area ^{40}Ar–^{39}Ar dating. Chin Sci Bull 44:2196–2199

Zhu B-Q, Mao C-X, Lugmair GW, MacDougall JD (1983) Isotopic and geochemical evidence for the origin of Plio-Pleistocene volcanic rocks near the Indo-Eurasian collisional margin at Tengchong, China. Earth Planet Sci Lett 65:263–275